Master's Thesis

Production of Rhombohedral Multilayer Graphene with the Goal of Making Diamane

Dong Ho Jeon

Department of Chemistry

Graduate School of UNIST

2019

Production of Rhombohedral Multilayer Graphene with the Goal of Making Diamane

Dong Ho Jeon

Department of Chemistry

Graduate School of UNIST

Production of Rhombohedral Multilayer Graphene with the Goal of Making Diamane

A thesis/dissertation
submitted to the Graduate School of UNIST
in partial fulfillment of the
requirements for the degree of
Master of Science

Dong Ho Jeon

01 / 07 / 2019 of submission
Approved by

_____

Advisor
Prof. Rodney S. Ruoff

Production of Rhombohedral Multilayer Graphene with the Goal of Making Diamane

Dong Ho Jeon

This certifies that the thesis/dissertation of Dong Ho Jeon is approved.

01 / 07 / 2019 of submission

signature

_____

Advisor: Prof. Rodney S. Ruoff

signature

_____

Prof. Hyun Suk Shin

signature

_____

Dr. Pavel V. Bakharev

Abstract

Multilayer graphene (MLG) is an outstanding anisotropic material whose electronic and mechanical properties are highly dependent on the stacking order of individual graphene monolayers. The most thermodynamically stable MLG configuration has a hexagonal crystal structure with an *ABA*…(Bernal) stacking sequence. Less energetically favorable and thus less abundant rhombohedral MLG with an *ABC*… stacking order is of a great interest due to its remarkable properties: electronic (tunable energy band gap) and structural (the same order of carbon layers as in the cubic diamond along [111] direction). It remains extremely challenging to synthesize MLG of an ABC stacking sequence by using 'bottom-up' approaches. To the best of our knowledge, there is only one report on the selective fabrication of ABC-stacked trilayer graphene by high-temperature annealing of n-type Si-terminated 6H-SiC(0001). The rhombohedral stacking order, however, has been reported to occur in natural graphite (up to 30%). Thus, in our attempt to make ABC-stacked MLG, we have chosen the 'top-down' approach, namely, by cleaving natural graphite with a relatively high content of the rhombohedral (*ABC*…) phase.

Throughout our study, we used X-ray diffraction (XRD) characterization to detect and to quantify the content of the rhombohedral phase in natural graphite. Hexagonal and rhombohedral phases in exfoliated MLG flakes were distinguished and mapped by Raman spectroscopy. We also conducted chemical functionalization (fluorination) of exfoliated graphene flakes to test the possibility of chemically induced sp^2 to sp^3 phase transition of ABC-stacked MLG into ultrathin diamond-like film (*diamane*).

Contents

LIST OF FIGURES

LIST OF TABLE

1. Introduction

Graphene is a truly two-dimensional (2D) material consisting of sp^2 hybridized atoms of carbon arranged in a hexagonal honeycomb lattice. Over the last decade intensive and extensive research has been conducted on single- and bilayer graphene to study their unique electronic, optical, mechanical, thermal, and chemical properties, among others. Multilayer graphene (MLG), including trilayer and thicker graphene films, has recently aroused a great deal of interest thanks to its exceptional anisotropic properties which are highly dependent on the stacking order of individual graphene sheets. Multilayer graphene films of the same thickness (i.e. with the same number of layers) but with different stacking orders show a significant difference in electronic transport and optical properties[1]. The hexagonal (*ABA*…) and rhombohedral (*ABC*…) are two the most stable crystallographic configurations. The hexagonal structure with an *ABA*… Bernal stacking sequence is slightly more thermodynamically stable than the *ABC*…stacking order. In 1964, Boehm H. P. and Coughlin R. W. conducted calorimetry to measure the enthalpy difference between rhombohedral and hexagonal phases in graphite.[2] The rhombohedral configuration which is less abundant bears a great interest for our research because it has the same layer order as in the cubic diamond along [111] direction.

One motivation for this research was our understanding that the diamond-like layer sequence in rhombohedral MLG is an essential (but not necessarily sufficient) prerequisite for chemically induced sp^2 to sp^3 phase transition from MLG to ultrathin diamond-like film. There are a number of theoretical (based on density functional theory) studies on the transformation of *ABC*-stacked MLG to diamond-like film (*diamane*) by chemical functionalization of the outer surface of MLG. Kvashnin *et al.*[3] reported the phase diagram in terms of pressure (*P*), temperature (*T*) and MLG thickness (*h*) obtained for diamane *vs*. *ABC*-MLG using *ab initio* computations of the Gibbs free energy. According to the calculated (*P,T,h*)-phase diagram, the effective pressure of the chemically induced phase transition from rhombohedral MLG of up to 8 layers thickness to diamane is negative. That means that the functionalization of the *ABC*-MLG outer surfaces may result in the formation of diamane without application of high pressures.

In general, various methods of synthesizing graphene can be subdivided into 'top-down' and 'bottom-up.' 'Top-down' methods include chemical and mechanical exfoliation of graphite while 'bottom-up' methods include chemical vapor deposition (CVD) and epitaxial growth on insulating surfaces (e.g. the surfaces of diamond and SiC). It remains extremely challenging to control not only the stacking order but also the number of layers using 'bottom-up' approaches. There is only one reported experiment on growing ABC-stacked trilayer graphene by high-temperature annealing of n-type Si-terminated 6H-SiC(0001).[4]

The hexagonal and rhombohedral phases often co-exist in natural graphite. It should also be

mentioned that Kish graphite and High Oriented Pyrolytic Graphite (HOPG) have the hexagonal stacking order of layers. It was also reported that the content of the rhombohedral modification can be increased by applying a mechanical milling (grinding) technique[5]. In that case shear forces generated by high energy milling can cause gliding of weakly interacting graphene sheets resulting in the formation of less energetically stable staking configurations (including ABC… stacking). Yet, the ball milling process may decrease the size of the crystallites significantly and thus induce amorphization of graphite samples.

In order to obtain *ABC*-stacked MLG, we have applied the 'top-down' approach, which means exfoliating natural graphite with a relatively high content (~30%) of the rhombohedral phase. The most common and straightforward method of graphite exfoliation is so called "Scotch-tape" method.[6] The modified "Scotch-tape" method to produce large area graphene flakes has been recently reported.[7] The main drawback of this method is that it was hard to control the number of layers, the yield and the quality. In our study we used this modified mechanical exfoliation method to produce relatively large MLG flakes of ABA… and ABC… stacking orders. The content of the rhombohedral phase in natural graphite has been estimated using X-ray diffraction (XRD) analysis. Raman spectroscopy was used to distinguish the hexagonal and rhombohedral layer sequences in the exfoliated MLG flakes.

2. Literature Review

2.1 Hexagonal and Rhombohedral Structure of Graphite

Hexagonal structure of graphite is the one of phase for natural graphite which stacked like *ABA* stacking sequence in their layers. Hexagonal graphite is the thermodynamically stable than rhombohedral graphite form in nature, most of graphite have the hexagonal structure as their stacked order. The crystallographic description of hexagonal graphite phase is given by the space group $D6h^4$-

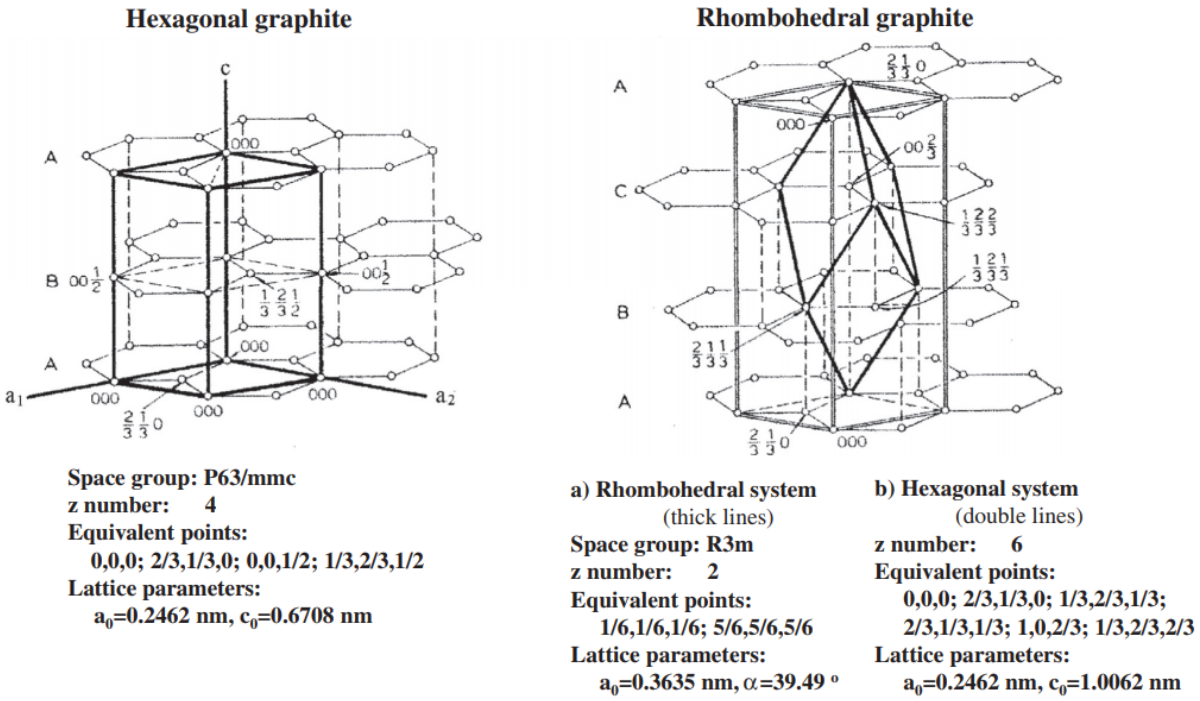

Figure 2.1 Crystal structure and lattice parameters of hexagonal graphite and rhombohedral graphite. (Reprinted with permission from reference **8**. Copyright 2013 *Elsevier* Inc.)

PG_3/mmc which has unit cell, a = 246.2 pm, c = 670.8 pm. In comparison to the hexagonal phase, rhombohedral phase is another phase of graphite which stacked like *ABC* stacking sequence in their layers. The crystallographic description of rhombohedral graphite phase is given by the space group D_3d^5-R^3m which has unit cell, a = 246.2 pm c = 1006.2 pm. **Fig 2.1** showed the crystal structure and lattice parameters of these two phases.[8] Most of natural graphite have both two phases but in case of artificial graphite like HOPG (Highly Oriented Pyrolytic Graphite) or Kish graphite, they display only small number of rhombohedral phase contents compared with hexagonal phase as a consequence of the thermodynamic stability.

Because of their different stacking order, the properties are slightly different each other. In 1964, Boehm *et al*,[2] measured the enthalpy difference, $\Delta \boldsymbol{H}$, between hexagonal and rhombohedral graphite as measuring the heat of formation of potassium graphite, C_8K. The experimental setup and measured formation energies are shown in **Fig. 2.2**. They used two kinds of graphite: 100% hexagonal phase

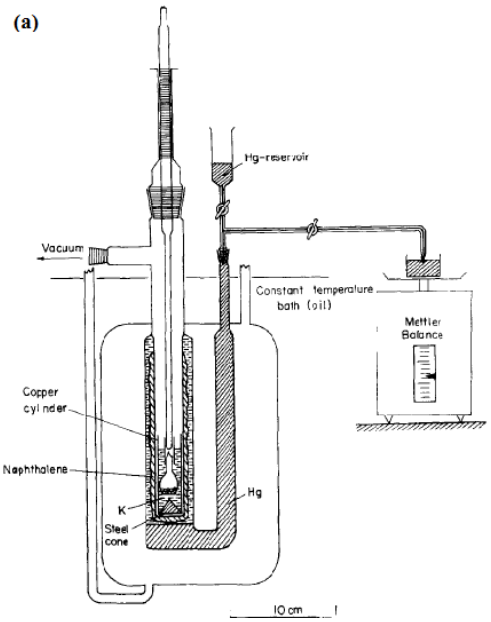

(b)

Sample	Reaction enthalpy ΔH
Hexagonal graphite:	
AF spezial, 3000°	84·2 cal/g
	83·6
	84·0
Madagascar flakes	84·0
	84·1
S40, soda	(84·9)* 84·5
	mean= 84·1 ±0·3 cal/g C
33% Rhombohedral graphite:	
AF spezial	87·1
	89·9
	86·8
	88·7
	88·0
	mean= 88·1 ±1·1 cal/g C

Figure 2.2 The experimental setup and the potassium graphite formation energies of two graphite phases.
(a) Instrumental setup for measuring formation energy (b) The formation energies depending on two phases. (Reprinted with permission from reference **2**. Copyright 1964 *Carbon*)

graphite which had been treated by high temperature for exchanging to fully hexagonal graphite and 33% rhombohedral graphite which had been treated by milling for increasing rhombohedral contents. They measured $\Delta \boldsymbol{H} = \boldsymbol{H}_{\text{rhom}} - \boldsymbol{H}_{\text{hex}} = 12.0 \pm 3.4$ cal / g **C** . For the comparison, we conducted the calculation for formation energies between two phase using DFT calculation method. As considering similar structures of two phases, the calculation data showed only 0.384 cal / g **C** as the theoretical formation energy. This unexpectable high experimental data was remarkable but the exact reason of high experimental value has not been revealed yet. For the detecting method of two phases, the best way to differentiate rhombohedral phase and hexagonal phase of graphite is X-ray diffraction (XRD) analysis which is shown in **Fig 2.3**.[9] The characteristic different peaks between hexagonal and rhombohedral phase are in 40 to 50 for 2θ region: Hexagonal (100), Rhombohedral (101), Hexagonal (101), and Rhombohedral (012) plane. From these distinctive 4 peaks, the rhombohedral contents in natural

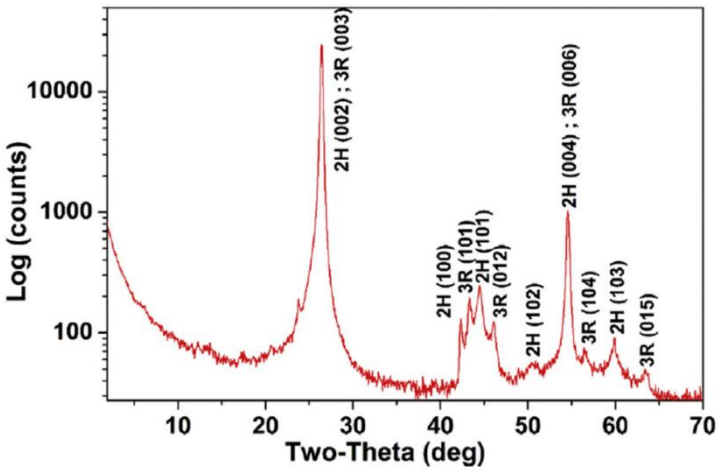

Figure 2.3 Typical Natural graphite X-ray diffraction patterns in 10 to 70 degrees 2θ region. (Graphite nanoplates) 2H indicates hexagonal phase peaks and 3R indicates rhombohedral phase peaks. (Reprinted with permission from reference **9**. Copyright 2017 *Carbon N. Y.*)

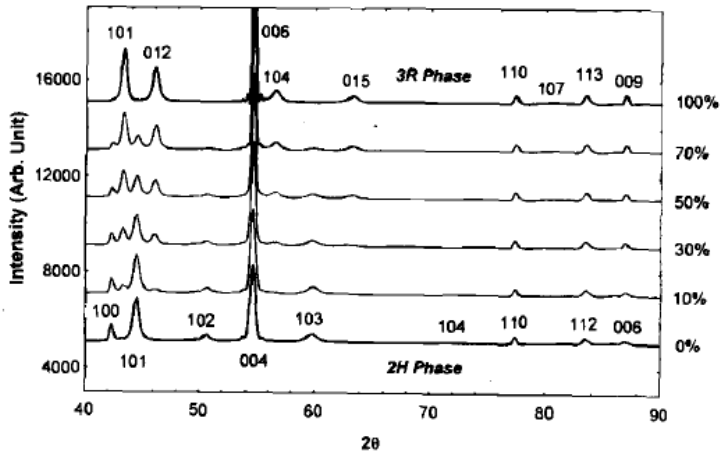

Figure 2.4 The XRD patterns which was calculated in depending on rhombohedral phase.
Left index indicated the rhombohedral contents. (Reproduced with permission from reference **10**. Copyright 1996 *J. Electrochem. Soc*).

graphite can be calculated by X-ray diffraction refinement calculation.[10] In these reference papers, they found that a tendency toward a higher rhombohedral phase content was observed when particle size of graphite was reduced. However, it was related to converting hexagonal phase to rhombohedral phase applying shear force not relationship between rhombohedral phase and particle size. For the evidence, they also found rhombohedral phase of two graphite in which the particle sizes are totally different.

Fig 2.4 is the calculation data of XRD patterns depending on rhombohedral contents.[10] As decreasing the hexagonal phase peak : H(100), H(101), it showed increasing rhombohedral peak : R(101), R(012). But in nature, because rhombohedral phase has the maximum contents 30%, actual XRD patterns is shown like **Fig 2.5** which is experimental XRD patterns of four different commercial graphite. From bottom to top, the rhombohedral content is increased from 0 to 30% in **Fig 2.5.** As it can be seen, the calculation data by XRD refinement procedure from rhombohedral contents (bracket

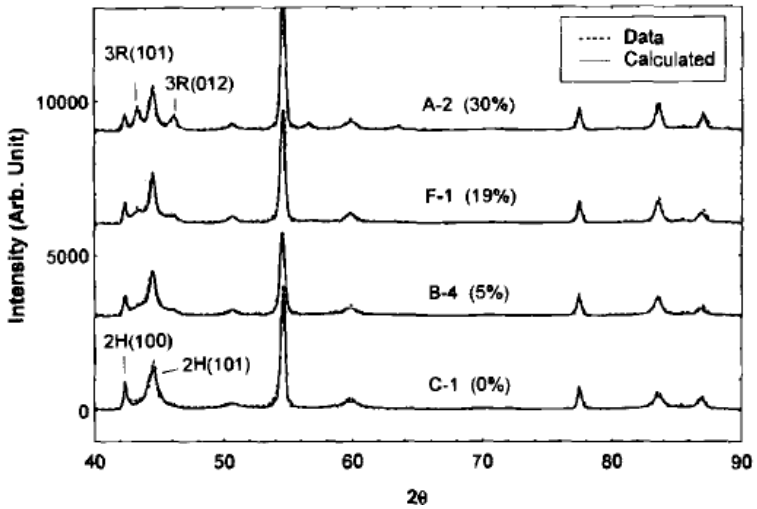

Figure 2.5 The XRD patterns of four different graphite. Bracket value is the rhombohedral phase contents
The solid line is calculation data and dotted line is experimental data which is exactly same as each other. (Reproduced with permission from reference **10**. Copyright 1996 *J. Electrochem. Soc*)

value) was well matched with experimental data.

2.2 Conversion to Rhombohedral phase of Graphite

From the enthalpy difference between rhombohedral phase and hexagonal phase, the conversion for two phases can be achieved by some treatments: ball-milling, grinding (hexagonal phase to rhombohedral phase) or heat treatment (rhombohedral phase to hexagonal phase). In 1956, E. Matuyama *et al*. published the paper which showed that the rate of transformation of rhombohedral graphite to hexagonal graphite at high temperature.[11] **Fig 2.6** is the XRD patterns for decreasing the rhombohedral peak which depended on the heating temperature from 1,000 to 1,800 ℃ for 1 hr. They calculated the integrated intensities of rhombohedral (101) peak and estimated the rhombohedral contents.

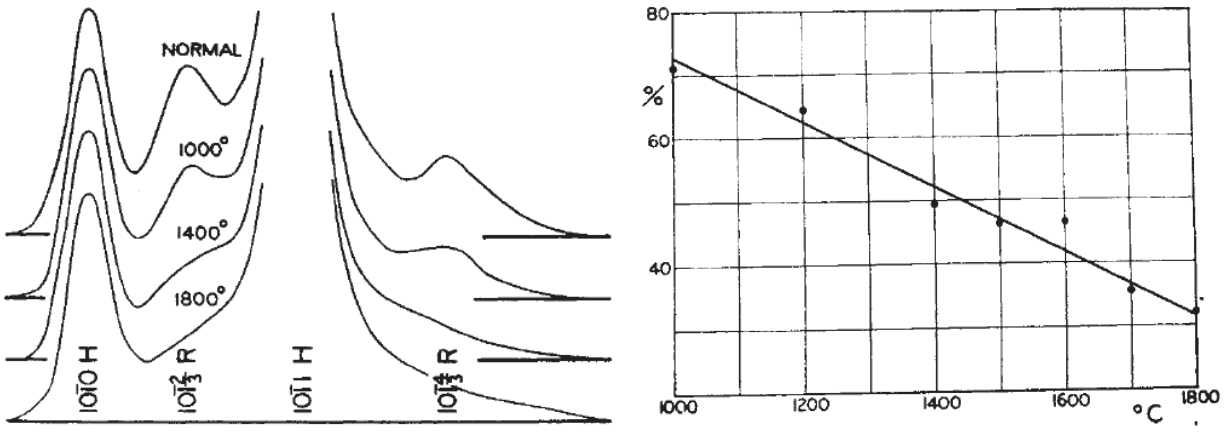

Figure 2.6 The XRD pattern depending on heating temperature near 40° 2θ region (Left figure). The line-plotted data for rhombohedral contents versus heating temperature (Right figure). The rhombohedral contents were calculated from intensity of rhombohedral (101) peak. (Reproduced with permission from reference **11**. Copyright 1956 *Nature*)

On the other hands, hexagonal phase simply converts to rhombohedral graphite by various grinding techniques. The conversion depends on grinding duration, atmosphere and even the kinds of grinding techniques. In general, the more increasing grinding duration, the layer structure of graphite is increased in their structure disorder, as well as the turbostraticity. So above certain point which randomness of structures exceed long-range order of structure, the graphite shows no longer long-ranged XRD pattern peak and it is close to the amorphous carbon. **Fig 2.7** shows the example of the conversion by using planetary and vibratory mill depending on milling atmosphere.[5] Compared with **Fig 2.7-a)** which is XRD pattern for as-received natural graphite well arranged by long-range order, **Fig 2.7-b) and c)** showed that the graphite structure was totally damaged by exceeding duration of milling. **Fig 2.7-d)** is for natural graphite milled in oxygen for 10 h in a planetary mill and they

showed the relative intensity of rhombohedral phase peak was increased. Basically, planetary and vibratory mill system have totally different energy delivery system to sample, so even though **Fig 2.7-b)** and **c)** have same milling atmosphere, two XRD patterns showed different peaks depending on their damaged structures.

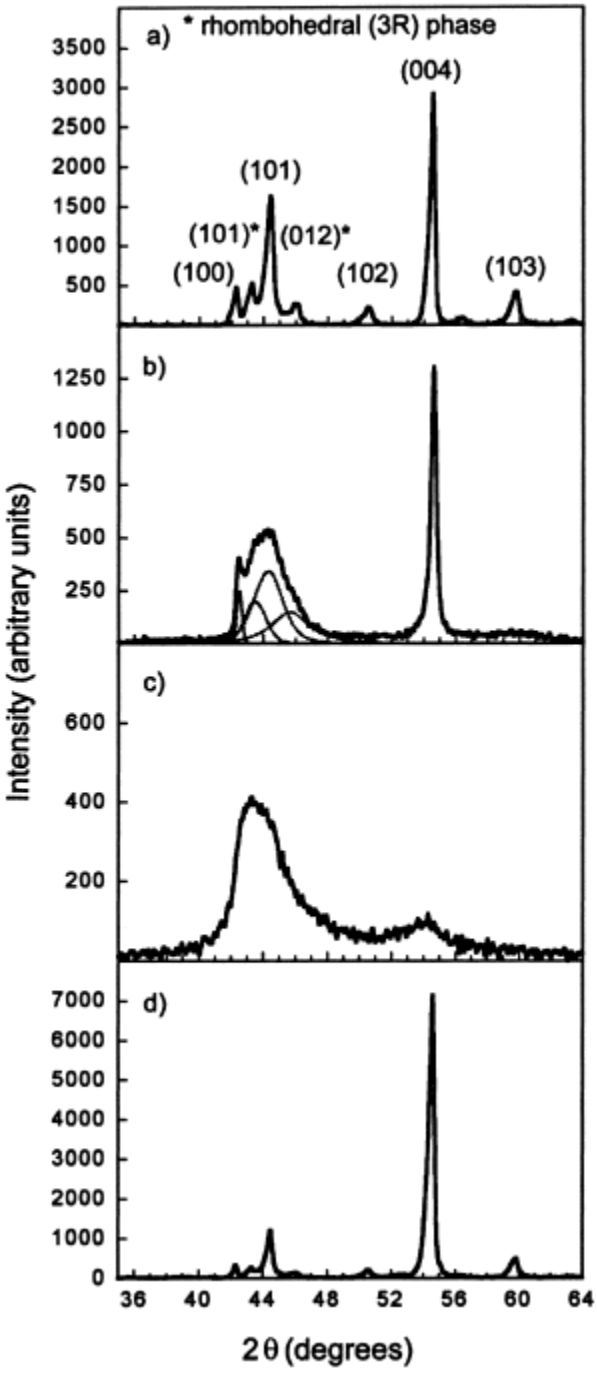

Figure 2.7 The XRD pattern for graphite which was applied by mechanical milling. a) as-received natural graphite b) natural graphite milled in an inert atmosphere for 3 h in a planetary mill c) natural graphite milled in an inert atmosphere for 3 h in a vibratory mill d) natural graphite milled in oxygen atmosphere for 10 h in a planetary mill. * mark indicates rhombohedral peak in XRD pattern.(Reproduced with permission from reference **5**. Copyright 2000 *Carbon*)

2.3 Mechanical Exfoliation of Graphite

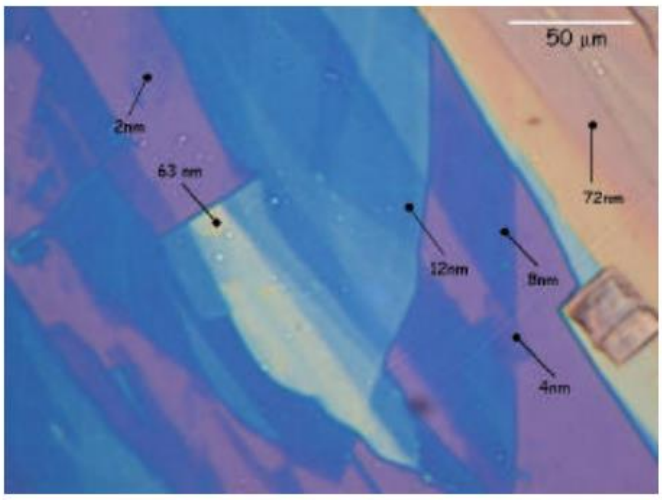

Figure 2.8 The exfoliated graphene on Si wafer for using HOPG. The thicker graphene showed brighter color than the thinner.(Reproduced with permission from reference **6**. Copyright 2004 *Science*)

The exfoliation of the graphite is commonly used in making the graphene as top-down approach because it is easier method to get the graphene than chemically synthesis of graphene. Firstly, Novoselov *et. al.* did the mechanical exfoliation of HOPG to make a graphene by using normal scotch tape and found the electrical property of few layer graphene.[6] **Fig 2.8** showed the exfoliated graphene which has the thickness from 2nm to 72nm measuring atomic force microscopy(AFM) analysis on SiO_2 substrate. From the information about the interlayer distance in bulk graphite about 0.34 nm thickness, they could estimate the graphene layer simply calculating from the thickness. The method is simple by using adhesive tape to split the graphite and easily obtaining the graphene, but the

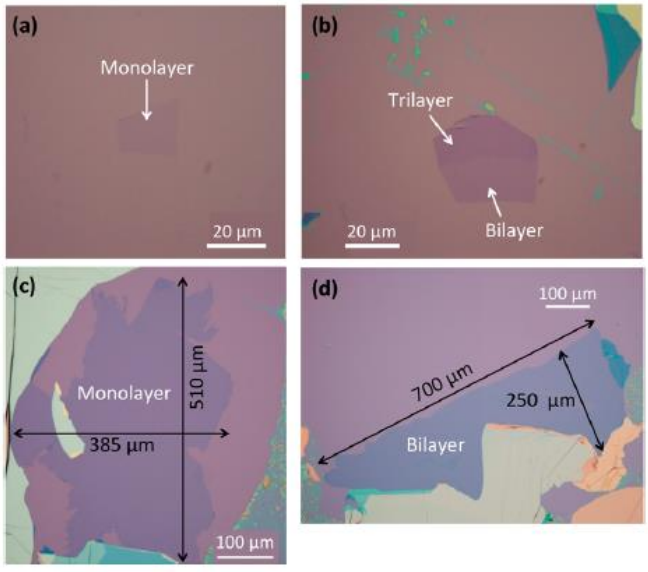

Figure 2.9 The optical microscopy image for the exfoliated HOPG using the normal and modified mechanical exfoliation method. Fig. (a) and (b) was previous results that their size was ~ 20 um^2 compared to Fig (c), (d) was the result for using modified method. (Reproduced with permission from reference **7**. Copyright 2011 *ACS nano*)

distribution of graphene layer is hardly controlled because of the difference for applying force when graphite is exfoliated. After that, Peter Sutter *et al.* modified the normal scotch tape method for obtaining large-area graphene other two dimensional materials.[7] Compared with the previous research for obtaining graphene which has various and uneven the size and layer, less than ~20 X 20 um^2, they obtained monolayer graphene that maximum size is ~ 500 X 350 um^2 (**Fig. 2.9**) and also they found the total graphene area was dramatically increased than previous mechanical exfoliation method. Key steps for the modified method were oxygen plasma and heat treatment for removing the adsorbates on SiO_2 substrate and controlling the pressure inside of graphene by applying heating process.

2.4 Raman Spectroscopy of Graphene

The Raman spectroscopy is a good technique to analyze the carbon materials. The basic principle of Raman spectroscopy is based on the light scattering process. When the monochromatic light is injected in the specific specimen, two kinds of light scattering are occurred: elastic scattering which is called Rayleigh scattering, and inelastic scattering which is called Raman scattering. Most phonons of injected light showed Rayleigh scattering that there is no exchange of energy between the atoms and light. However, because of molecules' own structures and atoms, Raman scattering is also occurred simultaneously which lose or gain the energy through the scattering process. Raman spectroscopy is detecting the energy difference between injecting light and scattering light.

Graphene has characteristic peaks in specific Raman shift and these peaks have deep relationship with their properties. **Fig. 2.10** showed normal Raman spectrum of graphene.[12] There are various peaks which can be possibly shown in graphene sample. However, in this study, it would discuss

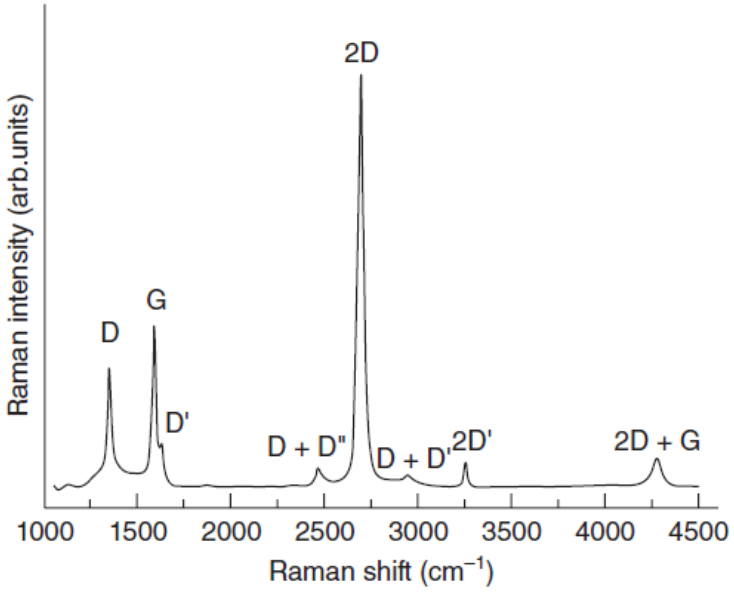

Figure 2.10 Raman spectrum of monolayer graphene with assignment of the Raman band. (Reproduced with permission from reference **12**. Copyright 2014 *Woodhead publishing*)

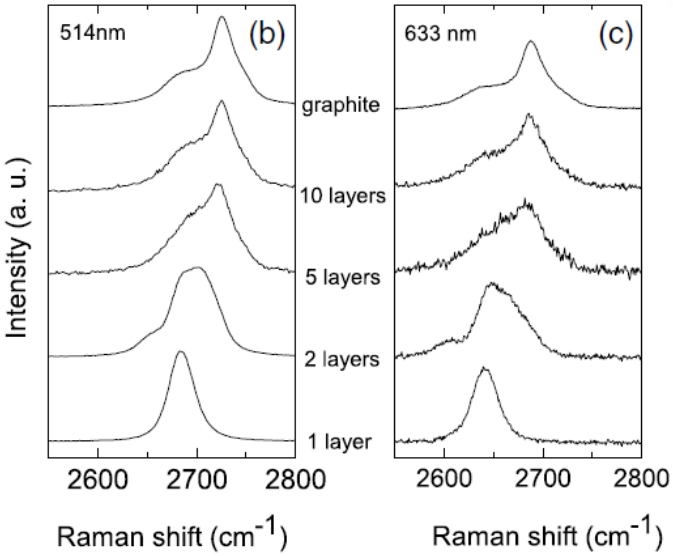

Figure 2.11 The 2D peak depending on the number of graphene layers.(Reproduced with permission from reference **15**. Copyright 2006 *Phys Rev Lett*)

about major 3 peaks: D peak, G peak, and 2D peak. Graphitic materials have one characteristic peak in 1580 cm^{-1} Raman shift which is called G peak came from the first-order Raman active mode. There are some reports that the position and shape of G peak can be changed by applying electronic or mechanical force like uniaxial strain to graphene.[13-14] The D peak is shown in 1350 cm^{-1} that it is related to the defect of graphene and functionalizing agents which are connected with carbon atom of graphene. The intensity of D peak shows the degree of defect in graphene. As the graphene is more damaged or functionalized, the intensity of D peak is increased. Of course, because of dangling bond in graphene edge, D peak is also shown in the edge of graphene. On the other hands, 2D peak which is came from double generated D peaks is in 2700 cm^{-1} is double for the position of D peak (1350 cm^{-1}). In case of multilayer graphene, 2D peak is good characteristic peak which can estimate the number of graphene layers.[15] **Fig. 2.11** is the data for the relationship between the number of layer and 2D peak. As the increase of the number of graphene layers, the 2D peak show the lower intensity than G peak

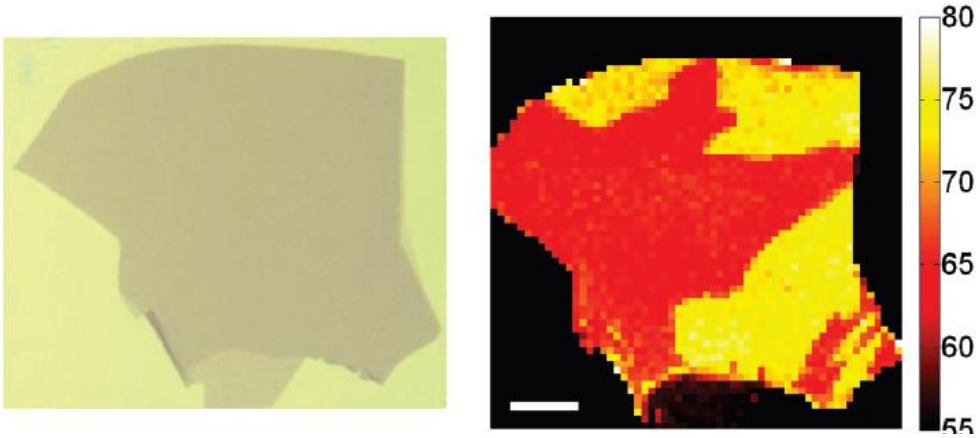

Figure 2.12 The optical image and spatial maps of the spectral width of Raman 2D peaks for trilayer graphene. Red and yellow region corresponds to ABC-stacked and ABA-stacked respectively. The scale bar is corresponded in 10 um. (Reproduced with permission from reference **16**. Copyright 2011 *Nano Lett*)

relatively. When the number of graphene layers is closed to graphite, the 2D peak is split to 2 peaks.

The shape of 2D peak is also related to their stacking order. In 2011, Tony F. Heinz *et al.*[16] showed the Raman imaging data depending on 2D line width based on previous research of IR experimental and calculation data for distinguishing ABA-stacked and ABC-stacked graphene (**Fig. 2.12**). After that, when it comes to the layer until 5 layers, Hyeonsik Cheong *et al.*[17] organized the comparison of 2D peak depending on the number of graphene layer and stacking order. They also found 2 minor peaks which can distinguish the stacking order of graphene like G^* peak (near 2450 cm^{-1}), M peak (near 1700 cm^{-1}) but 2D shape is more clearly seen than other minor peaks. **Fig. 2.13** is the 2D peak data for few-layer graphene with two different stacking orders under five different excitation energies. We used the point that the shape of 2D peak is different for excitation wavelength and in case of 2.33 eV, ABC-stacked multilayer graphene shows more higher peak than ABA-stacked multilayer graphene in lower Raman shift about 2680 cm^{-1}.

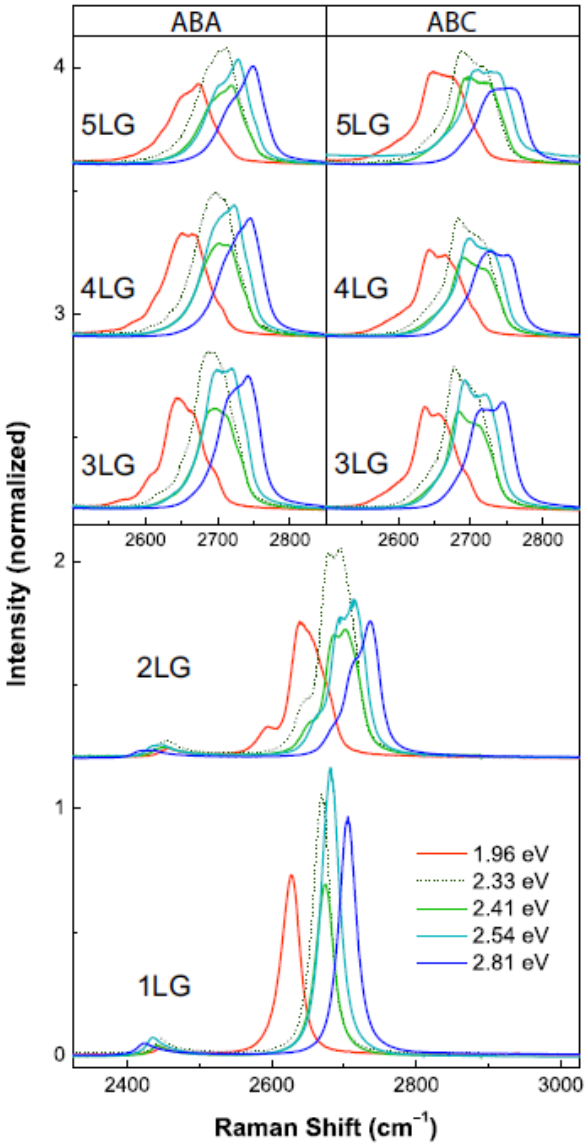

Figure 2.13 2D peak of few-layer graphene with 2 different stacking order under 5 different excitation energies. (Reproduced with permission from reference **17**. Copyright 2014 *Sci Rep*)

2.5 Conversion of multilayer graphene to Diamane

Basically, the graphene is composed to sp^2 carbon layer compared with diamond which is composed to sp^3 carbon network because the graphene is one layer detached graphite. The conversion of graphite to diamond is the one of desirable part for many researchers. Although the people found the conversion applying high pressure and high temperature, this artificial diamond is need to high costs because of harsh synthetic condition. After remarkable discovery of graphene, researchers considered

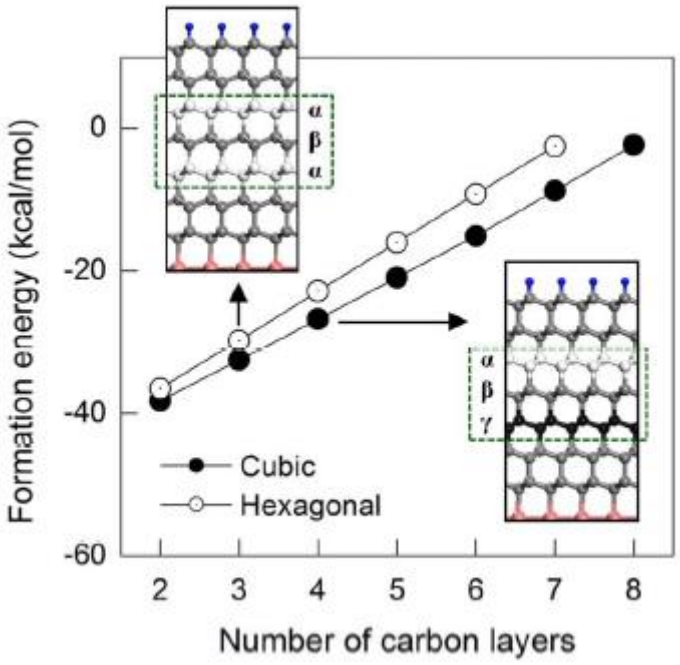

Figure 2.14 The formation energy of diamane depending on the number of layer and stacking order of multilayer graphene. The negative value of the formation energy showed the stability of diamane. (Reproduced with permission from reference **18**. Copyright 2013 *Sci Rep*)

another conversion which simply functionalize the graphene in order to convert sp^2 to sp^3 carbon bond. There were several calculation papers about the possibility for synthesis of diamond, or diamond-like structures through this chemically induced conversion. **Fig 2.14** showed the formation energy of diamane structures depending on graphene's stacking order and the number of graphene layers.[18] Until 8 layers, functionalized multilayer graphene showed the minus formation energy

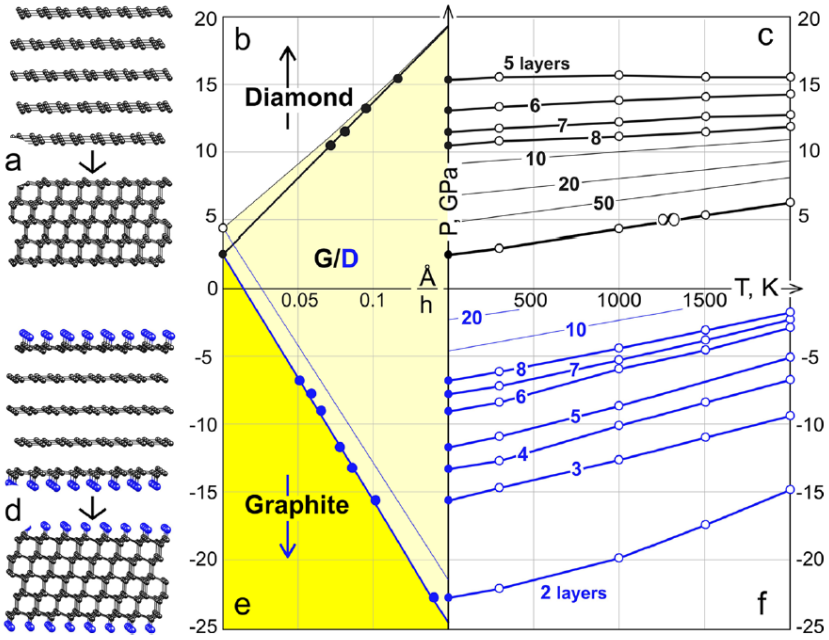

Figure 2.15. The scheme when multilayer graphene is converted into diamond with or without chemically induced procedure and phase diagram in terms of Pressure(P), Temperature(T), and MLG thickness(h). (Reproduced with permission from reference **3**. Copyright 2014 *ACS nano*)

which means the thermodynamically stable structures. They assumed the multilayer graphene on metal foil, Co(0001) and the functionalization source is hydrogen. Compared that AA-stacked graphene can make the hexagonal structure of diamond which marked their layers as αβ, ABC-stacked graphene can make the cubic diamond-like structure which marked their layers as αβγ.

Kvashnin et al.[3] reported the phase diagram in terms of three parameter: Pressure (P), Temperature (T), and MLG graphene thickness (h) compared between diamane versus ABC-stacked MLG using *ab initio* computations of Gibbs free energy. **Fig. 2.15** showed the phase diagram for making the diamond structures using n-layer graphene with or without chemically induced procedure. In case of ABC-stacked MLG without any functionalization, it need to high pressure which is positive phase transition pressure in diagram. But when the hydrogenation is conducted in ABC-stacked MLG, the film transformation into diamond form doesn't require pressure at all (the equilibrium line corresponds to $P < 0$ until 8 layers).

3. Experimental Section

3.1 Mechanically Exfoliation of Natural Graphite.

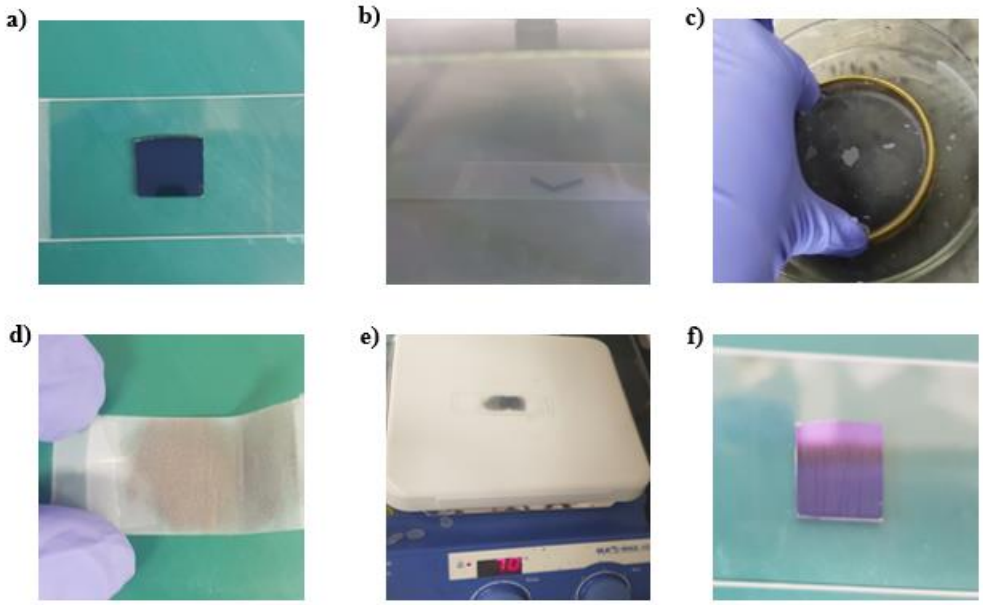

Figure 3.1 The procedure of exfoliation for natural graphite. a) Si / SiO_2 which has 300 nm oxide thickness, b) Oxygen plasma treatment c) Filtration of natural graphite d) exfoliated graphite on scotch tape e) heat treatment using conventional heating plate f) exfoliated graphene on Si wafer.

For obtaining multilayer graphene which has high contents of rhombohedral stacking order (ABC-stacked), we exfoliated the natural graphite which has about 30% rhombohedra contents (Sigma Aldrich, -325 mesh). we repeated the modified mechanical exfoliation using the natural graphite powder following the procedure (**Fig. 3.1**).[7] we prepared Si / SiO_2 substrate which has 300 nm oxide layer and to get rid of adsorbates I treated oxygen plasma in 10 ppm oxygen concentration atmosphere for 10 minutes. We also conducted the sonication procedure to filter the natural graphite in a DI water bath in order to increase the size of the exfoliated graphene using the metal sieve (450 mesh, 34 um hole size). After that, I selected the bigger size graphite which was in upside of the mesh than normal graphite powder. The exfoliation was done by using normal scotch tape, but additional heat treatment was conducted because of enhancing the adhesive between Si wafer and exfoliated graphene. The heating condition was 70 ℃ for 5 min. After cooling, the scotch tape was detached from the substrate. The multilayer graphene had average size about 10 um. **Fig. 3.2** is optical microscopy images for obtaining the exfoliated graphene through this procedure. There were also thick graphite flakes (black arrow), and partially exfoliated graphite (blue arrow) coexist with multilayer graphene.

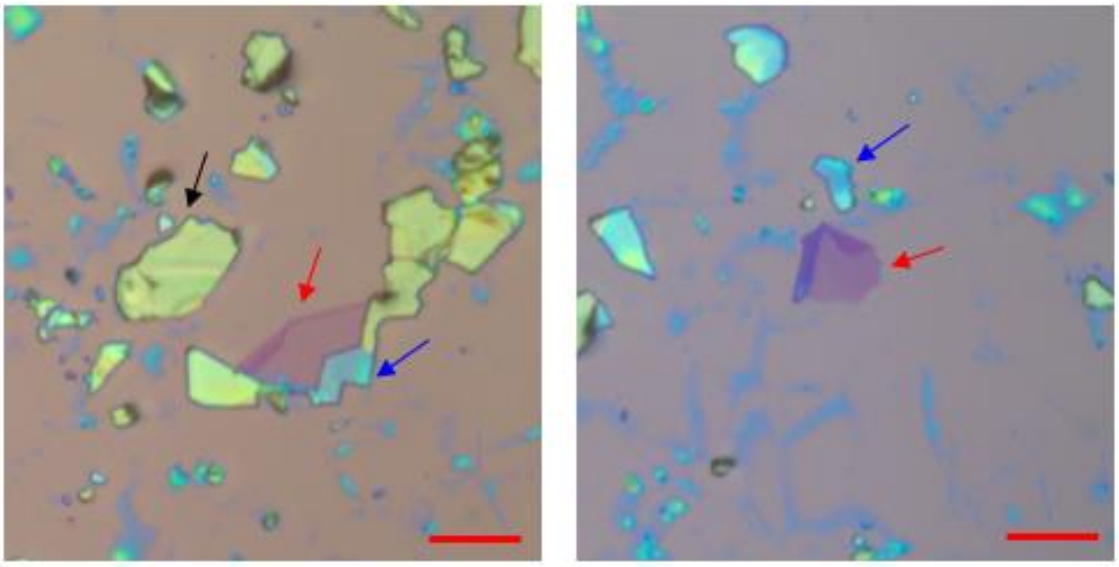

Figure 3.2 Optical microscopic images of exfoliated multilayer graphene. The scale bar is 10 um and red, blue, black arrow indicate the multilayer graphene which has 2~3 layers, above 10 layers, graphite flakes respectively.

3.2 Raman Analysis

In order to distinguish the layer stacking order of multilayer graphene, Raman spectroscopy was used with a Wi-Tec micro Raman instrument using 488nm(2.54 eV), 532 nm(2.33 eV) laser excitation with a spot size of 250 nm. For the Raman mapping, I measured single spectrum of desired multilayer graphene for 60 x 60 spots with 1 s integration time, but total measured time was depending on the multilayer sample size.

3.3 XRD Analysis

X-ray diffraction (XRD) analysis was for measuring the rhombohedral contents of natural graphite. Rigaku SmartLab powder X-ray diffractometer was used in XRD analysis by using Cu-Kα source (λ = 0.154 nm) through Cu-Kβ filtration. The bragg angle range was fixed in 30 to 60 degree because there are two rhombohedral characteristic peaks compared with two hexagonal characteristic peaks. The reference data of rhombohedral and hexagonal phase of graphite was obtained by International Centre for Diffraction Data (ICDD).

3.4 AFM Analysis

Bruker Dimension Icon atomic force microscope was used for AFM analysis for checking the number of multilayer graphene. AFM measurement range was 10 X 10 um for scan rate 0.88 Hz. The number of multilayer graphene was calculated by the information about one layer of graphene that is 0.34 nm which is the calculation data for interlayer distance of graphite.

3.5 Fluorination of Multilayer Graphene

For the functionalization of multilayer graphene, I used the home-built system for fluorination (**Fig 3.3**). The fluorine source was XeF_2 source which has the vapor pressure ~ 3.8 Torr at ambient atmosphere. Because of enhancing the fluorination for the sample, the chamber was retained in 60 Celsius degree by heating elements. Liquid nitrogen was used as the trap agent for removing harmful fluorine gas.

Figure 3.3 The home-built system of fluorination

3.6 XPS Analysis

X-ray photoelectron spectroscopy (XPS, Thermo Scientific ESCALAB 250 Xi) was used to confirm the fluorination of multilayer graphene/graphite flakes on SiO_2 substrate and as-received graphite powder.

4. Results and Discussion

4.1 Characterization

4.1.1 XRD Analysis

Basically, the rhombohedral contents of natural graphite strongly affect the mechanical treatment. We used the commercial natural graphite powder which has – 325 mesh (below 45 um). **Fig 4.1** is the XRD patterns of natural graphite depending on ball milling. The ball milling condition is 150 rpm to

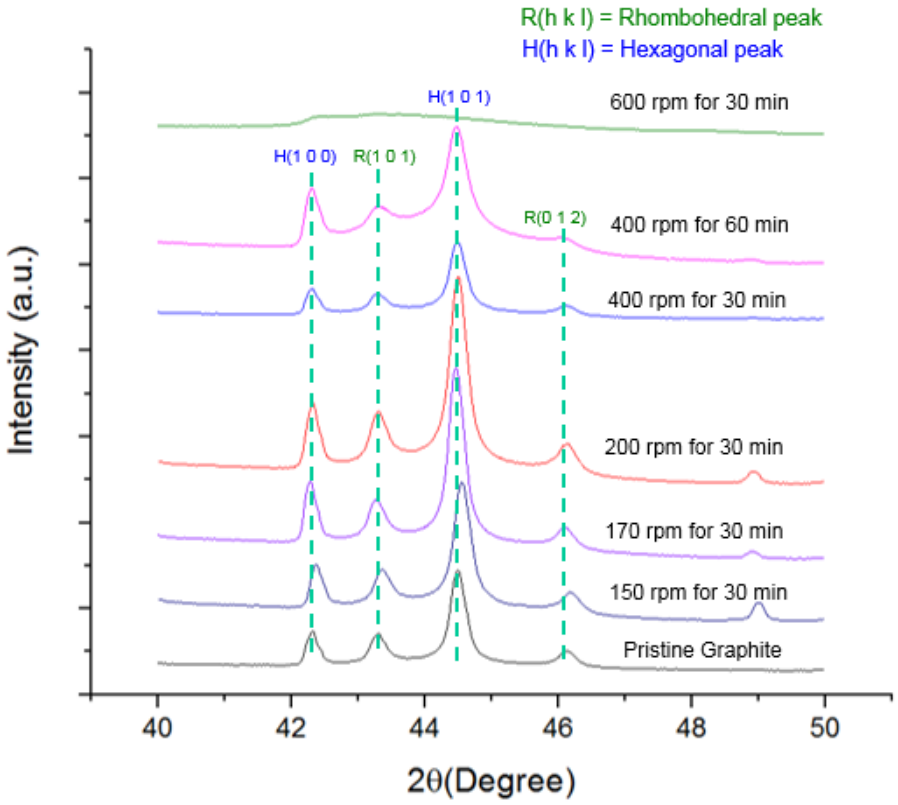

Figure 4.1 The XRD pattern for natural graphite depending on ball-milling condition.

600 rpm in ambient atmosphere by using planetary ball milling system. **Table 1**. is the data for the calculation of area ratio between rhombohedral and hexagonal peaks and full-width half maximum (FWHM) of rhombohedral (101) peak as the fitting first order Lorenzian function. They had the general trend for increasing the ratio of hexagonal and rhombohedral phase leaded from applying mechanical force. But also, FWHM of rhombohedral (101) peak gradually increased because of damaging for the graphite structures. It means the ball-milling process effect to increase the rhombohedral phase but also damage the graphite structures. Especially, the 400 rpm condition had more broaden base line than below 400 rpm condition and above 600 rpm, crystallinity were totally broken. The estimated rhombohedral contents of graphite are around 30 % which is closed to maximum contents of that in natural graphite. We guess that it leads from refinement procedure that

natural graphite powder already underwent the milling process using jaw-crusher in order to make the specific particle size.

Milling Condition	The area ratio $S_{R(101)} / S_{H(101)}$	FWHM of R(101)
Pristine	0.32	0.28
150 rpm	0.30	0.32
170 rpm	0.33	0.34
200 rpm	0.33	0.38
400 rpm	0.34	0.41
600 rpm	-	-

Table 1. The area ratio between R(101) and H(101) and FWHM of R(101) peaks depending on milling condition.

The average grain size of rhombohedral stacked graphite along [101] direction can be calculated to use Scherrer's equation as well known for crystallite calculation equation:

$$L_{R(101)} = \frac{K \times \lambda}{B \times \cos \theta_B}$$

where the K is shape factor, 0.91 in case of graphite, λ is the wavelength of X-ray source and B is FWHM of rhombohedral (101) in Bragg angle θ_B. The average grain size of rhombohedral stacked graphite is about 30.6 nm but as the increase of milling duration, FWHM of rhombohedral (101) is also increased so, the grain size is decreased.

4.1.2 AFM Analysis

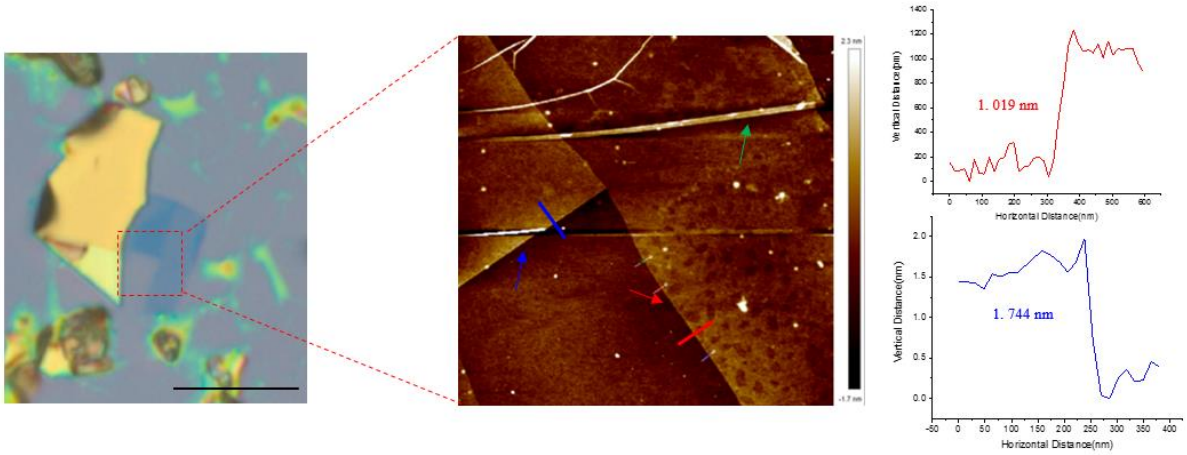

Figure 4.2 The optical microscopic and AFM image of multilayer graphene. The red and blue arrow indicate trilayer and five layers region respectively. The green arrow indicates the folding the graphene region during exfoliation. The scale bar is 10 um.

In case of mechanical exfoliation of natural graphite, the number of graphene layer is totally random, but we can estimate the number of layers through the contrast of graphene in optical microscopy

image. **Fig. 4.2** is the optical microscope image and AFM measurement image. The gold color in optical microscope image means closed to the graphite layers. Based on the optical microscope image, we can measure the exact thickness by AFM analysis. The marked value in image is the calculated value through the one-layer thickness is about 0.34 nm. Because the mechanical exfoliation by using scotch tape can't clearly detach the graphite layer so some spots showed that folding or twisting the graphene layer. (**Fig. 4.2**, green marked) It means that the stacking order also can be different within the graphene flakes. However, the stacking order cannot be detected by optical microscopic image or AFM measurement. There is no relationship between the stacking order and AFM measurement image or optical microscopic image.

4.1.3 Raman Spectroscopy

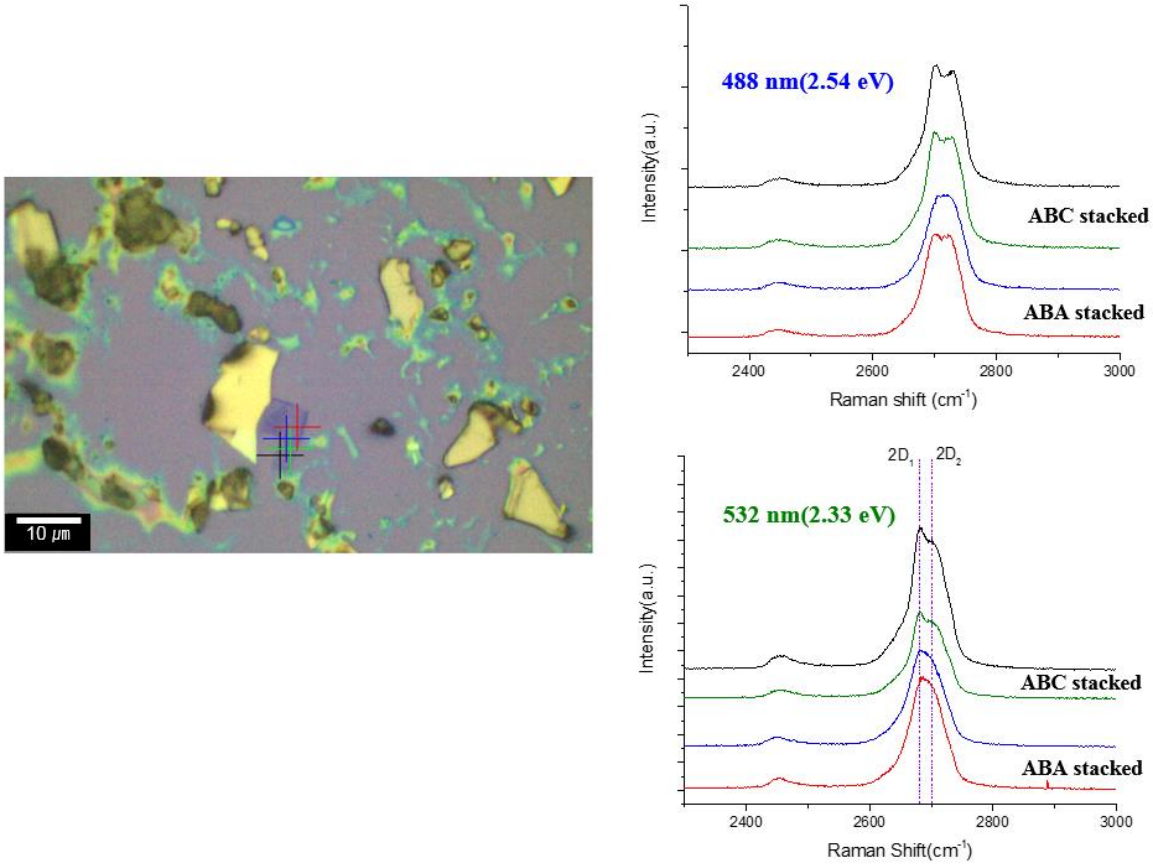

Figure 4.3 Single Raman spectrums of multilayer graphene. We marked $2D_1$ and $2D_2$ which is in 2670 cm^{-1}, 2700 cm^{-1} respectively in case of 2.33 eV (532 nm) excitation wavelength. The color of spectrum and cross mark in optical microscopic image mean each spectrum correspond each position. Red and blue mark is ABA stacked and green, black mark is ABC stacked.

We can distinguish between ABA-stacked graphene and ABC-stacked graphene following reference paper.[17] The ABC-stacked graphene showed the higher peak in 2D peak region (~2700 cm^{-1}) than the ABA- stacked graphene. **Fig. 4.3** is showed the single Raman spectrum between ABA-stacked and ABC-stacked multilayer graphene. We marked $2D_1$ and $2D_2$ within 2D band to distinguish the

stacking order. In case of 2.33 eV (532nm) excitation wavelength, we assigned that $2D_1$ is the subpeak of 2D in 2670 cm^{-1} and $2D_2$ is in 2700 cm^{-1}. For the visualization of stacking order, we calculated the ratio between the intensity of $2D_1$ and $2D_2$ in whole graphene region. We can see three situations for their stacking order through this calculation: Dominantly ABC, ABC + ABA and dominantly ABA-stacked within same graphene region (**Fig. 4.4**). The brighter color in mapping data is closed to ABC-stacked order and the darker color is closed to ABA-stacked. Totally black region means the graphite because the graphite showed 2D splitting with dramatically lower $2D_1$ peak than $2D_2$. Because we

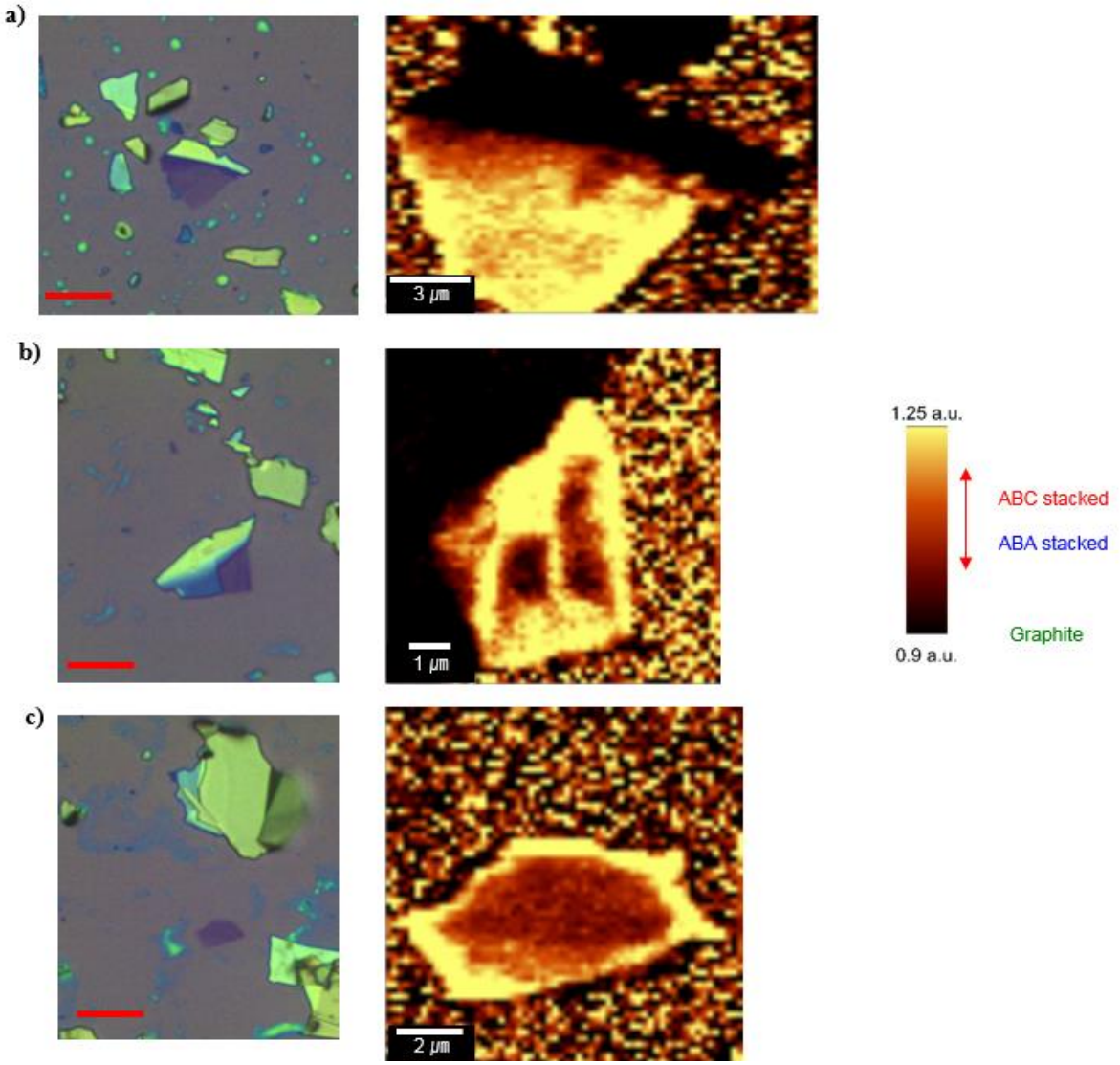

Figure 4.4 Raman mapping images in terms of the ratio between $2D_1$ and $2D_2$ peak. In optical microscopic image, all scale bar indicates 10 um. Raman mapping scale bar is same range 0.9 to 1.25 a.u. a) dominantly ABC stacked b) both ABA and ABC stacked exist c) dominantly ABA stacked.

calculated the "ratio" in whole multilayer graphene region, the outside of the graphene region also showed the "color spot", but it should be noticed that the outside of graphene and edge side of graphene should be ignored as we were checking the stacking order of graphene. The stacking order was not changed by the Raman monochromatic laser through several scanning.

4.2 Fluorination of Multilayer Graphene

Through our home-built fluorination system, we functionalized the multilayer graphene on Si wafer directly. The successful fluorination of the exfoliated MLG/graphite flakes on the SiO_2 surface was confirmed by the X-ray photoelectron spectroscopy (XPS). The high resolution C1s spectra of as-received graphite powder as well as the high resolution C1s and F1s spectra of the exfoliated graphene/graphite flakes fluorinated on the SiO_2 surface are shown in **Fig 4.6**. **Fig 4.6 (a)** shows a single asymmetric peak at 284.3 eV corresponding to the sp^2 hybridized carbon atoms with a $\pi \rightarrow \pi^*$ transition feature at ~290.7 eV. After fluorination of MLG and thin graphite flakes which were exfoliated onto the SiO_2 surface, the XPS revealed the formation of C-F covalent bonds as indicated

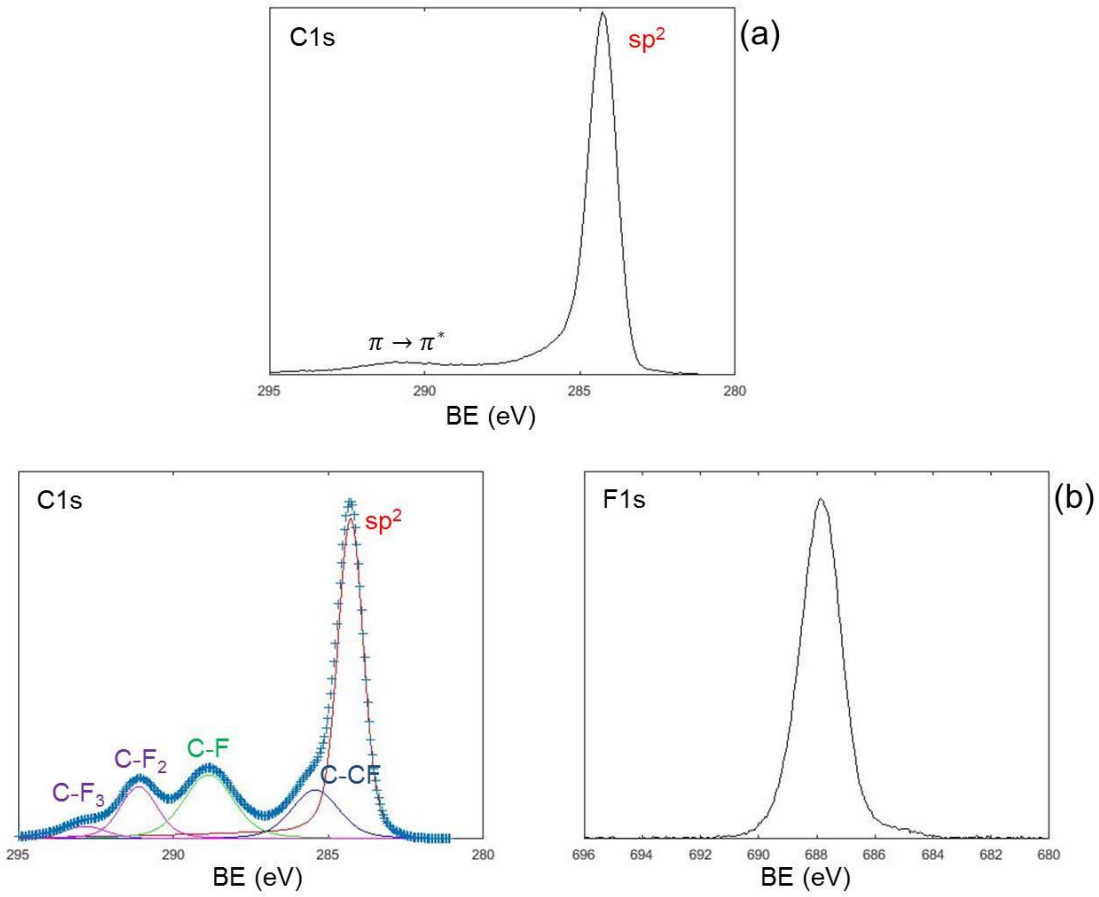

Figure 4.6 The XPS data for as-received graphite and fluorinated MLG/graphite flakes on SiO_2 surface. (a) C1s spectra of as-received graphite and (b) C1s and F1s spectra of fluorinated MLG/graphite flakes on SiO_2 surface

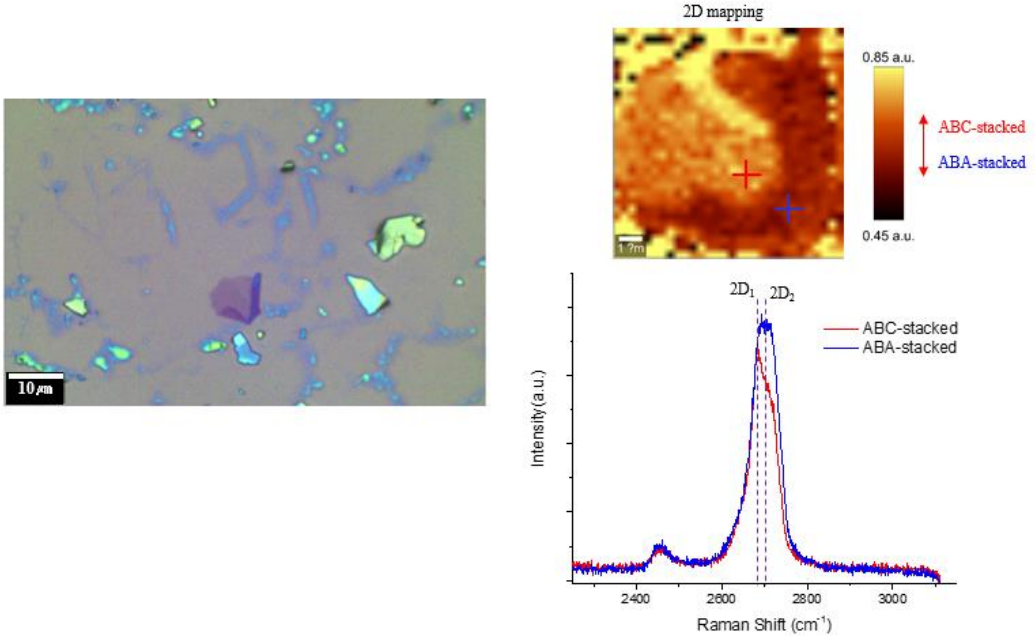

Figure 4.7 The Raman spectrum before fluorination. The darker field mean ABA-stacked graphene region within 2D mapping of the sample. Single spectrums showed the ABA-stacked and ABC-stacked graphene 's 2D shapes.

by the prominent peaks in the corresponding C1s spectrum and a covalent signal in the F1s spectrum.

Before the fluorination, we checked the stacking order of multilayer graphene (**Fig. 4.7**). The darker field means ABA-stacked graphene compared with the brighter field. When we fluorinated multilayer graphene 1st time as exposure to XeF_2 source, the graphene showed the functionalized graphene peak that because of fluorine, the intensity of D peak was increased and lower G peak and 2D peak. But inside of center of multilayer graphene, they showed relatively bigger G peak than edge of the multilayer graphene and simultaneously D' peak is shown which is related to D peak and defect in

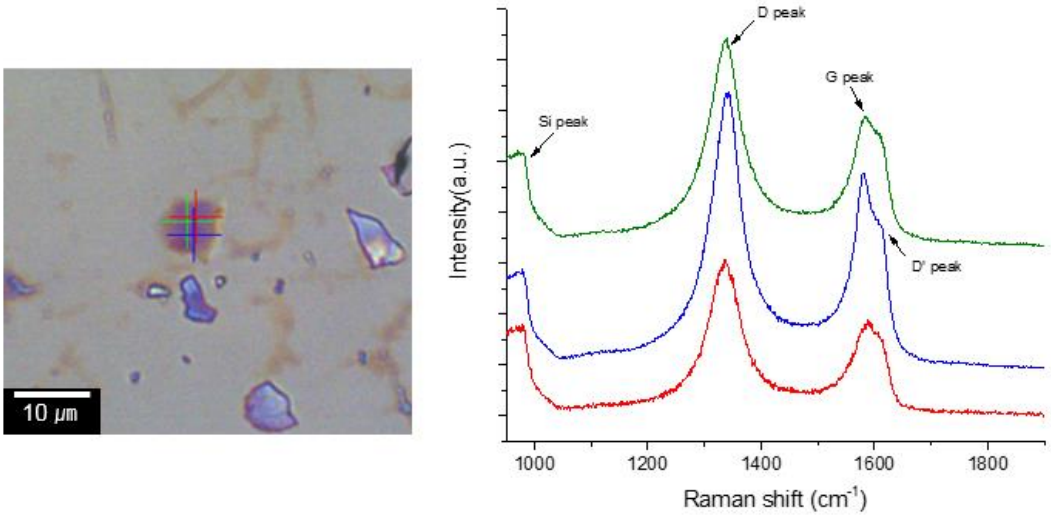

Figure 4.8 The Raman spectrum of 1st fluorinated multilyaer graphene. The same color means the same position in optical image.

1620 cm^{-1}.(**Fig. 4.8**) It means the center of the multilayer graphene wasn't fully functionalized and the color also "graphene" color in optical microscopy but it was slightly blurred. After 2nd exposure which applied the sample in harsher condition than 1st exposure, the multilayer graphene showed totally optically transparency like the monolayer fluorographene. The transparency is the characteristic property of fully fluorinated monolayer graphene. But in the Raman spectrum (**Fig. 4.9**), there is no big difference between ABA-stacked (Blue mark) and ABC-stacked graphene (Red and green mark). We guess two possibilities of this functionalized multilayer graphene that one is the multilayer fluorographene which fluorinated layer by layer and the other is closed to diamane structure. However, for the proving of their structures, we need to the detail analysis for that structure including the TEM / EELS measurement.

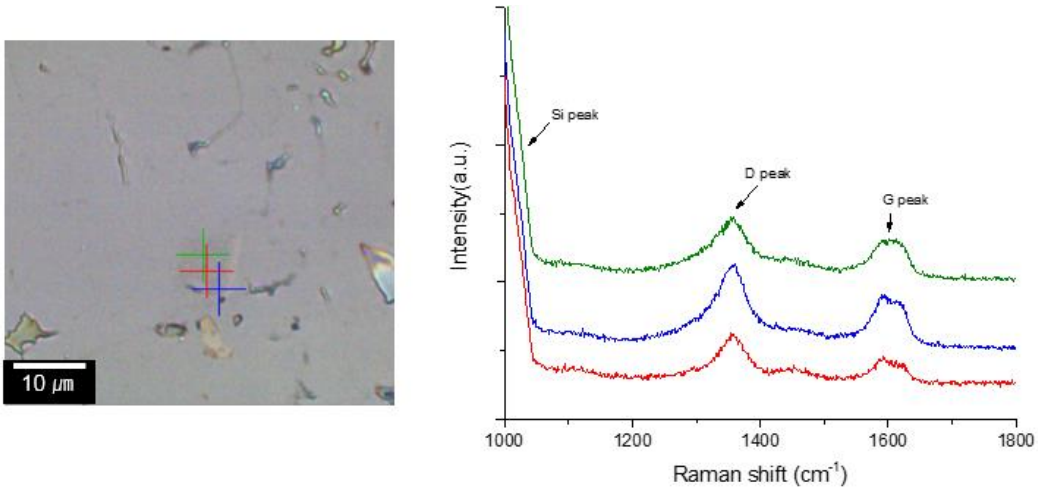

Figure 4.9 The Raman mapping data before fluorination and Raman spectrum of 2nd fluorinated multilayer graphene. The same color also means the same position in optical image. Red and green site is ABC-stacked graphene, blue site is ABA-stacked graphene which was checked by Raman spectrum before fluorination.(**Figure 4.6**)

5. Conclusion

Here, we studied the production of rhombohedral multilayer graphene with checking the stacking order by using the Raman spectroscopy. Firstly, we chose the commercial natural graphite which has high contents of rhombohedral phase by checking the XRD characterization. The natural graphite has about 30% rhombohedral phase. Through the filtration, we selected larger size of natural graphite and conducted mechanical exfoliation using the modified scotch tape method. For distinguishing the rhombohedral and hexagonal phase in multilayer graphene, we used the Raman spectrum of multilayer graphene which showed the different 2D peak shape depending on their stacking order. So, we could find three kinds of graphene region with respect to two stacking order: Dominantly Rhombohedral phase (ABC-stacked), Coexist rhombohedral and hexagonal phase (ABC + ABA stacked), and hexagonal phase (ABA-stacked). We visualized as the Raman mapping by calculating the ratio between $2D_1$ and $2D_2$ which were two subpeaks of 2D peak. For the chemical functionalization, we fluorinated multilayer graphene using our homebuilt system in order to test the possibility of chemically induced sp^2 and sp^3 phase transition of ABC-stacked multilayer graphene in to ultrathin diamond-like films called Diamane. The interesting part of results is that as more exposing the fluorine source (XeF_2), the whole multilayer graphene region showed optically transparent which is well-known property for fluorographene which is fluorinated monolayer graphene. We considered two kinds of possibilities: One is multilayer fluorographene and the other is ultrathin diamond-like structure. So, for the deep analysis of their structure, we plan to the functionalization with hydrogen and TEM measurement for analyzing the structures.

REFERENCE

1. Mak, K. F.; Shan, J.; Heinz, T. F., Electronic structure of few-layer graphene: experimental demonstration of strong dependence on stacking sequence. *Phys Rev Lett* **2010,** *104* (17), 176404.
2. Boehm, H. P.; Coughlin, R. W., Enthalpy difference of hexagonal and rhombohedral graphite. *Carbon* **1964,** *2* (1), 1-6.
3. Kvashnin, A. G.; Chernozatonskii, L. A.; Yakobson, B. I.; Sorokin, P. B., Phase Diagram of Quasi-Two-Dimensional Carbon, From Graphene to Diamond. *Nano Letters* **2014,** *14* (2), 676-681.
4. Sugawara, K.; Yamamura, N.; Matsuda, K.; Norimatsu, W.; Kusunoki, M.; Sato, T.; Takahashi, T., Selective fabrication of free-standing ABA and ABC trilayer graphene with/without Dirac-cone energy bands. *Npg Asia Materials* **2018,** *10*, e466.
5. Ong, T. S.; Yang, H., Effect of atmosphere on the mechanical milling of natural graphite. *Carbon* **2000,** *38* (15), 2077-2085.
6. Novoselov, K. S.; Geim, A. K.; Morozov, S. V.; Jiang, D.; Zhang, Y.; Dubonos, S. V.; Grigorieva, I. V.; Firsov, A. A., Electric Field Effect in Atomically Thin Carbon Films. *Science* **2004,** *306* (5696), 666-669.
7. Huang, Y.; Sutter, E.; Shi, N. N.; Zheng, J.; Yang, T.; Englund, D.; Gao, H.-J.; Sutter, P., Reliable Exfoliation of Large-Area High-Quality Flakes of Graphene and Other Two-Dimensional Materials. *ACS Nano* **2015,** *9* (11), 10612-10620.
8. Inagaki, M., Advanced Carbon Materials. 2013; pp 25-60.
9. Seehra, M. S.; Geddam, U. K.; Schwegler-Berry, D.; Stefaniak, A. B., Detection and quantification of 2H and 3R phases in commercial graphene-based materials. *Carbon N Y* **2015,** *85*, 818-823.
10. Shi, H.; Barker, J.; Saïdi, M. Y.; Koksbang, R., Structure and Lithium Intercalation Properties of Synthetic and Natural Graphite. *Journal of The Electrochemical Society* **1996,** *143* (11), 3466-3472.
11. Matuyama, E., Rate of Transformation of Rhombohedral Graphite at High Temperatures. *Nature* **1956,** *178*, 1459.
12. Hulman, M., 7 - Raman spectroscopy of graphene. In *Graphene*, Skákalová, V.; Kaiser, A. B., Eds. Woodhead Publishing: 2014; pp 156-183.
13. Das, A.; Pisana, S.; Chakraborty, B.; Piscanec, S.; Saha, S. K.; Waghmare, U. V.; Novoselov, K. S.; Krishnamurthy, H. R.; Geim, A. K.; Ferrari, A. C.; Sood, A. K., Monitoring dopants by Raman scattering in an electrochemically top-gated graphene transistor. *Nature Nanotechnology* **2008,** *3*, 210.
14. Mohiuddin, T. M. G.; Lombardo, A.; Nair, R. R.; Bonetti, A.; Savini, G.; Jalil, R.; Bonini, N.; Basko, D. M.; Galiotis, C.; Marzari, N.; Novoselov, K. S.; Geim, A. K.; Ferrari, A. C., Uniaxial strain in graphene by Raman spectroscopy: G peak splitting, Gr\"uneisen parameters, and sample

orientation. *Physical Review B* **2009,** *79* (20), 205433.

15. Ferrari, A. C.; Meyer, J. C.; Scardaci, V.; Casiraghi, C.; Lazzeri, M.; Mauri, F.; Piscanec, S.; Jiang, D.; Novoselov, K. S.; Roth, S.; Geim, A. K., Raman spectrum of graphene and graphene layers. *Phys Rev Lett* **2006,** *97* (18), 187401.

16. Lui, C. H.; Li, Z.; Chen, Z.; Klimov, P. V.; Brus, L. E.; Heinz, T. F., Imaging stacking order in few-layer graphene. *Nano Lett* **2011,** *11* (1), 164-9.

17. Nguyen, T. A.; Lee, J. U.; Yoon, D.; Cheong, H., Excitation energy dependent Raman signatures of ABA- and ABC-stacked few-layer graphene. *Sci Rep* **2014,** *4*, 4630.

18. Odkhuu, D.; Shin, D.; Ruoff, R. S.; Park, N., Conversion of multilayer graphene into continuous ultrathin sp(3)-bonded carbon films on metal surfaces. *Sci Rep* **2013,** *3*, 3276.

ACKNOWLEDGEMENT

Firstly, I would like to thank my thesis advisor Prof. Dr. Rodney S. Ruoff, Distinguished Professor, Chemistry Department, Ulsan National Institute of Science and Technology(UNIST) for introducing the diamane research topic and for his kind guidance. His direction and passion have always encouraged me during this diamane research. He is also director of Center for Multidimensional Carbon Materials (CMCM), Institute for Basic Science (IBS), so he gave me many advices and efforts that it can be possible to achieve this works. This work wouldn't have been possible without his helps and encouragement.

I express my sincere thanks to our lab colleagues of CMCM who assisted me in this research. Especially, Dr. Pavel V. Bakharev who is research fellow in our group, gave me lots of comments and advices as my mentor. From I came our laboratory, he teaches lots of things as not only my mentor of this research but also my friend.

I also want to thank to following member: Dr. Dulce Camacho, Dr. Sun Hwa Lee, Dr. Wonkyoung Sung, Dr. Sunghwan Jin, Dr. Da Luo, Dr. Ming Huang, Meihui Wang, Chongyang Zhu, Min gu, Jaehong Seo, Sangjun Oh, Hyunju Nam, helped me about instrumental techniques and experimental skills in this research. I remember that when I first came here, they helped me for adapting to our laboratory.

I would like to thank my last committee member, Prof. Dr. Hyunsuk Shin for spending time to evaluate my graduation thesis and watch my defense presentation.

Lastly, I must thank to my parents, two older sisters and friends for their encouragement and supporting. Their warm words and assists always give me the motivation in my life.